Applied Geochemistry 63 (2015) 93–104

Contents lists available at ScienceDirect

Applied Geochemistry

journal homepage: www.elsevier.com/locate/apgeochem

Modeling past and present activity of a subarctic hydrothermal system using O, H, C, U and Th isotopes

A.I. Malov [a, *], I.N. Bolotov [a], O.S. Pokrovsky [a, b, c], S.B. Zykov [a], I.V. Tokarev [d], Kh.A. Arslanov [e], S.V. Druzhinin [a], A.A. Lyubas [a], M.Y. Gofarov [a], I.A. Kostikova [f], V.V. Kriauciunas [a], S.B. Chernov [e], F.E. Maksimov [e], Yu.V. Bespalaya [a], O.V. Aksenova [a]

[a] Institute of Environmental Problems of the North of the Ural Branch of Russian Academy of Sciences, 23 Severnoy Dviny Emb., Arkhangelsk, 163061, Russia
[b] GET, CNRS, UMR 5563, Observatoire Midi-Pyreneés, 14 Avenue Edouard Belin, Toulouse, France
[c] BIO-GEO-CLIM Laboratory, Tomsk State University, Tomsk, 634050, Russia
[d] Resource Center "Geomodel", Research Park, Saint-Petersburg State University, 1 Saint-Petersburg, 198504, Russia
[e] Faculty of Geography and Geoecology, Saint-Petersburg State University, 33 10th Line, V.O., Saint Petersburg, 199187, Russia
[f] Sergeev Institute of Enviromental Geoscience of the Russian Academy of Sciences, 13, Build. 2 Ulansky per, Moscow, 101000, Russia

ARTICLE INFO

Article history:
Received 13 September 2014
Received in revised form
20 June 2015
Accepted 10 July 2015
Available online 3 August 2015

Keywords:
Groundwater dating
Radiocarbon
Travertine
Uranium and thorium isotopes

ABSTRACT

The hot springs of the Pymvashor subarctic hydrothermal system are of considerable interest because the area is devoid of recent volcanism and is located in the permafrost region. We attempted to evaluate the activity of thermal waters with respect to host rocks to quantify the water residence time in this system and date the associated travertine. Therefore, we used the chemical composition of the thermal waters, thermodynamic modeling, $\delta^{18}O$ and $\delta^{2}H$ labels and isotopes, such as ^{14}C–$\delta^{13}C$, ^{234}U–^{238}U, and ^{230}Th–^{232}Th. The $\delta^{18}O$ and $\delta^{2}H$ values indicated the infiltration of atmospheric water in the recharge area of the hydrothermal system and suggested a stable paleoclimate in the area over the last 5–7.9 thousand years. The fresh water flows through deep parts of the aquifer system where it mixes with brine followed by discharge. The hot springs geothermal water total dissolved solid (TDS) ranged from 1.8 to 2 g/L, and in the deep wells, the TDS ranged from 7.1 to 198 g/L. The ratios of Na/Cl (mol), $Br/10^{-3}Cl$ (ppm), and Ca/Cl (ppm) in the thermal springs ranged from 0.89 to 0.90, 1.8 to 1.9, and close to 0.12, respectively, reflecting participation of deep brines in their formation. The composition of the thermal water can be formed via a mixture of one part of the brines with 130 parts of the cold water end member with a TDS of 291 mg/L. The results of thermodynamic modeling and mixing diagram analysis indicate that during water–rock interaction in the aquifer, the precipitation of calcite and the dissolution of gypsum and magnesite were accompanied by hydrolysis of the sodium aluminosilicates with precipitating clay secondary minerals. The low uranium concentration in the Pymvashor groundwater (0.24–0.34 ppb) and the sufficiently long water residence time combined with the relatively high $^{234}U/^{238}U$ activity ratios (3–5) suggest a high α recoil loss and low dissolution rates of the host rocks or a high precipitation rate and adsorption of uranium. The elevated values of the α recoil loss may be due to radioactive decay of the precipitated and adsorbed ^{238}U because in this case, the probability of ^{234}Th release and ^{234}U appearance in water increases ~4-fold compared to the probability of emission directly from the rock. The ^{14}C age of the water was estimated to be between 4960 and 7870 years, and the $^{230}Th/U$ age of the travertine ranged from 1970 to 7650 years. Overall, these results allow for a better understanding of the nature and evolution of the thermal waters in this unique subarctic hydrothermal system.

1. Introduction

Important geothermal areas are scattered throughout northern Eurasia. These areas are primarily associated with regions of recent volcanic activity (Laverov et al., 2006; Kovalenko et al., 2009). However, some geothermal areas are also located in non-volcanic

* Corresponding author.
E-mail address: malovai@yandex.ru (A.I. Malov).

http://dx.doi.org/10.1016/j.apgeochem.2015.07.003
0883-2927/

regions associated with deep faults, especially in upland areas and near the foothills of mountains. All hydrothermal systems function due to an ascent of hot water to the surface along the fracturing zone. Heating of the water occurs either due to a rise in the magma to relatively shallow depths (Kiryukhin et al., 2012; Afsin et al., 2014; Mimura et al., 1995; Fournier, 1989) or a geothermal gradient (Mayrhofer et al., 2014; Busby, 2014; Kamel, 2012; Mohammadi et al., 2010). For the heated water to ascend to the surface, the hydrostatic pressure in the hydrothermal system must be lower than the surrounding pressure. These conditions are met due to the lower density of the heated fluid and the lower hypsometric position of the sources at the Earth surface. The heated water ejected on the surface is replaced by fresh water from the watershed divides in a similar fashion to the water inflows to the wells or the groundwater input to lakes, rivers and seas. A portion of this fresh water penetrates to greater depths, becoming a hot end member of the geothermal system, and another portion of this fresh water joins the shallow subsurface water reservoir, reducing the temperature of the hot water. The water is also mobilized from the higher depths. However, its proportion is believed to be relatively small because the filtration properties of rocks are typically significantly reduced at depth (Fig. 1).

The typical but little-known geothermal area known as Pymvashor has several hot springs and is located at the Chernyshev Hill Ridge in northeastern Europe (Bogolitsin and Bolotov, 2011) (Fig. 2).

The high-latitude geothermal habitats of live organisms form a very different environment than non-geothermal areas (O'Gorman et al., 2012). According to some authors (Pleshanov et al., 2002; Bogolitsin and Bolotov, 2011; Bolotov et al., 2012; Pointing et al., 2014), these geothermal areas may play important roles as warm refugia for fresh water organisms. The hydrochemical data of the Pymvashor sources are very limited (Vollosovych and Knyazev, 1956; Mityusheva et al., 2011), and there is no information

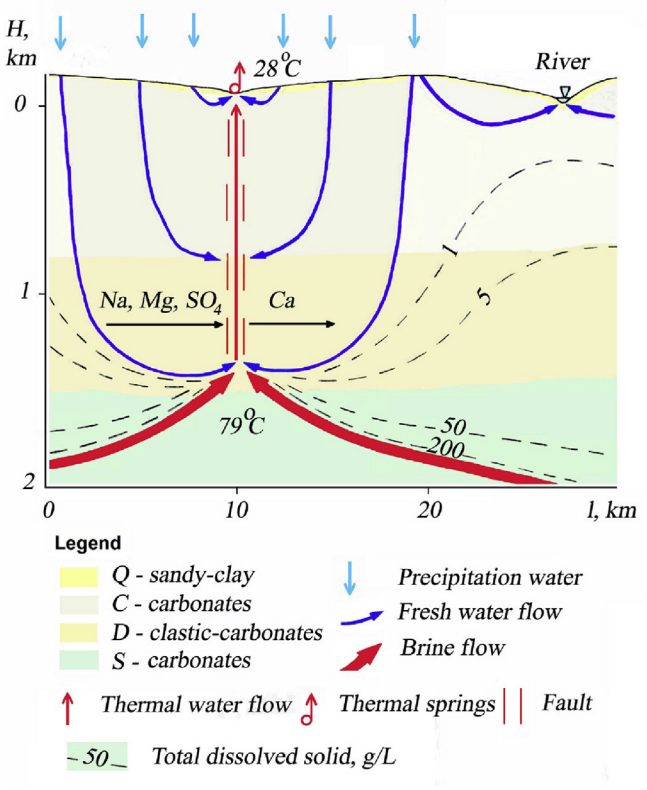

Fig. 1. Conceptual model of the hydrothermal system Pymvashor.

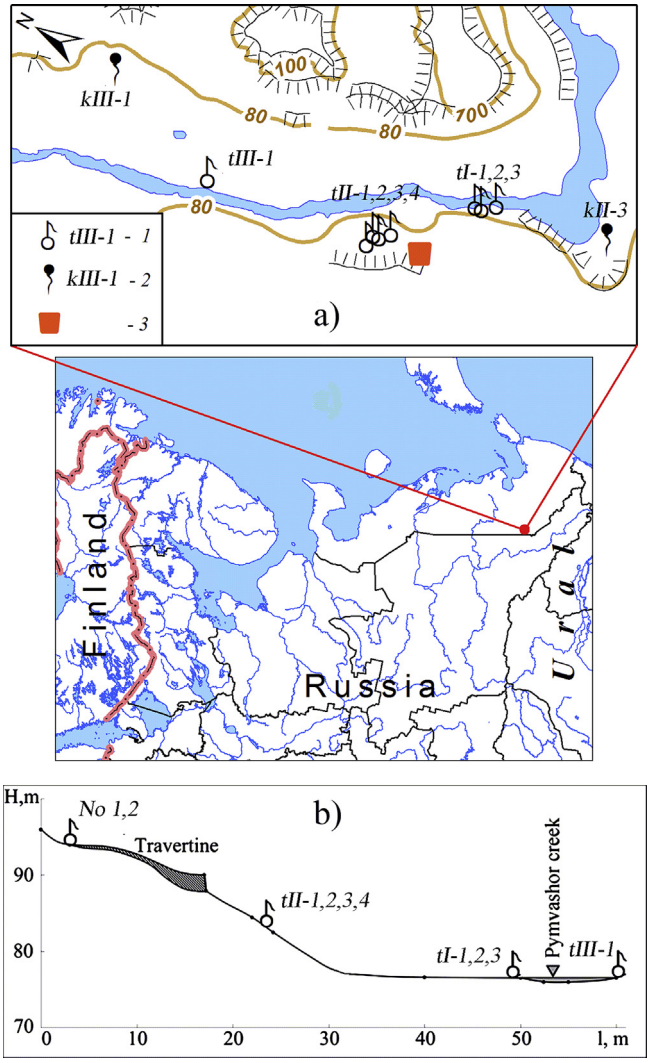

Fig. 2. General location of the study site showing the sampling locations (a) and the structure of the slope of the river valley with high-rise location springs and travertine (b). *1* – thermal spring with its number; "No 1,2" in Fig. 1 b) are non-functioning springs; *2* – cold spring with its number; *3* – travertine.

available on the isotopic composition of the thermal waters and travertine.

The objective of this study was to obtain the chronological estimates and data necessary for the reconstruction of the paleoecological environments of the subarctic hydrothermal system during the late Pleistocene and Holocene. In particular, we aimed to test different isotopic chronometers to evaluate the age of the water and travertine in this hydrothermal system. Therefore, we measured the isotopic (i.e., δ^2H, $\delta^{18}O$, $\delta^{13}C$, ^{14}C, $^{234}U/^{238}U$, $^{230}Th/U$) and chemical characteristics.

To estimate the ^{14}C residence time of groundwater in the aquifer, we used the flow piston model (Münnich, 1957, 1968). This model assumes uniform groundwater movement along a flow line without consideration of diffusion and dispersion of solutes (Supplementary Information S1). This model takes into account isotopic dilution and exchange processes in unsaturated zones and aquifers that can alter $^{14}C_0$ (i.e., Ingerson and Pearson, 1964; Pearson and Hanshaw, 1970; Fontes and Garnier, 1979; Han and Plummer, 2013).

The use of ^{234}U and ^{238}U has been extensively employed to infer the chronological constraints on the fluid residence times (Osmond

and Cowart, 1976, 1982; Andreas and Kay, 1983; Ivanovich et al., 1991; Fröhlich et al., 1991; Fröhlich, 2013; Maher et al., 2004, etc.). In this study, we have refrained from using uranium isotopes for groundwater dating due to the limited number of estimating points along the groundwater flow. However, the isotopic composition of water reflects the balance between the α recoil effect and the dissolution rate of the host rocks (Andrews et al., 1982; Fröhlich and Gellermann, 1987). The host rocks and minerals retain the equilibrium $^{234}U/^{238}U$ activity ratio when they were not subjected to recent alterations by physical or chemical processes, such as grinding or leaching (i.e., remain monolithic). The rocks in the aquifers partially lose intermediate U decay products due to the α recoil effect when the ^{238}U atom decay is accompanied by α particle ejection, and the produced recoil ^{234}Th atom is ejected in the opposite direction. If the decay occurs near the rock–liquid interface, this atom enters the water and rapidly transformed to ^{234}U. Due to this process, the $^{234}U/^{238}U$ activity ratio decreases compared to its equilibrium value, and the groundwater appears to be enriched with excessive ^{234}U isotope (Cherdyntsev, 1955; Chalov, 1969). In the solid phase, this effect is most notable during sediment deposition and its diagenesis in the slightly lithified state, where the porosity of this sediment is as high as 0.7 (Maher et al., 2004). For mud- and clay-sized particles (65–1 μm), the loss of ^{234}U during fractionation varies from a few percent to 50% (DePaolo et al., 2006). Simultaneously, the relative ^{234}U loss for large grains and their aggregates is low, and an equilibrium activity ratio equal to 1 is remains unchanged in sediments and rocks. The increase in the $^{234}U/^{238}U$ activity ratio in groundwater that comes into contact with host rocks regardless of their grain size is substantially higher because the U concentration in water is typically two to four orders of magnitude lower compared to that in rocks and an additional ^{234}U atom provides for its growth by 100 to 10,000 times. The aquifers are characterized by $^{234}U/^{238}U$ values reaching 10–20 (Ivanovich et al., 1991; Porcelli, 2008; Malov, 2013). If the solid phase is simultaneously dissolved, water receives uranium characterized by a low $^{234}U/^{238}U$ value (~1), and the activity ratio decreases to <2–5. Therefore, the isotopic composition of water reflects the balance between the α recoil effect and the dissolution rate of the host rocks. A higher $^{234}U/^{238}U$ ratio results in a lower the dissolution rates of rocks and vice versa. A lower U concentration in water results in a lower dissolution rate of rocks or shorter interaction in the water–rock system or higher precipitation rate and adsorption of uranium. A higher U concentration in water results in higher dissolution of rocks and a longer interaction between the water and the rocks (Supplementary Information S2).

In addition, according to Ivanovich et al. (1991, p. 406–407), "Uranium isotope studies of many aquifers from outcrop to confined, deeper regions have resulted in identification of redox zones leading to classification of discrete aquifer regimes (Osmond and Cowart, 1982; Andreas and Kay, 1983; Cuttell et al., 1986). These are (1) the oxidizing part characterized by high U content and moderate $^{234}U/^{238}U$ activity ratios (the augmenting regime); (2) a redox barrier characterized by very low U content and high $^{234}U/^{238}U$ activity ratios; and (3) deep aquifer regimes recognizable by constant, low U content and steady decrease of the $^{234}U/^{238}U$ activity ratio with time, or depth (the decaying regime) … Consequently, U content in groundwaters is very sensitive to redox conditions, resulting in large variations from 0.001 to more than 100 μg/kg (Osmond and Cowart, 1976, 1982)".

In oxidized bicarbonate-rich natural waters, U is present as a uranyl–carbonate complex. In contrast, Th^{4+}, which is easily hydrolyzed, precipitates or adsorbs on clay particles. Therefore, travertines precipitated from groundwater contain significantly more U than Th. However, due to the decay of uranium, ^{230}Th accumulates. Therefore, from the $^{230}Th/^{234}U$ and $^{234}U/^{238}U$ activity ratios, the age of the travertine can be determined (Kaufman and Broecker, 1965) (Supplementary Information S3).

Using this multiple hydrochemical and isotopic approach, the age and evolution of the Pymvashor high-latitude hydrothermal system have been evaluated for the first time using comparisons of different pairs of isotopes.

2. Overview and geological structure

Pymvashor thermal springs are located within the Chernyshev Ridge, a large structure at the junction of the Pechora plate of the East European Platform and the Pre-Urals Foredeep (Fig. 2). The occurrence of Paleozoic rocks is shown in Fig. 3b and c: limestone, dolomite (S, C), limestone, dolomite, magnesite, gypsum, marl, shale, carbonaceous clay, sandy limestone (D), and mudstone, siltstone, and marl (P). The Chernyshev Ridge formed in $T_3 - J_1$ on a system of faults in a basement under compression (Derevyanko and Zharkov, 1987). In the Jurassic period, the appearance of subintrusive bodies was accompanied by eruptions of central volcanoes. In Mikulian times (mQIIImk) approximately 130–115 ka ago, marine accumulation occurred in depressed areas of relief. During the Pleistocene glaciation approximately 90 ka ago, this area was located outside of the ice sheet and is presumed to have been covered by the waters of the huge ice dammed reservoir, named Lake Komi (Astakhov et al., 1999; Mangerud et al., 2004; Svendsen et al., 2004). When the lake drained, contemporary river valleys and watersheds formed and thermal springs appeared on the land surface. Currently the entire territory is covered by Pleistocene deposits up to 50 m thick. The exception is the neotectonic uplift near the thermal springs in Pymvashor creek valley. Here, outcrops of carbonate rock of the Lower Carboniferous (C_1), and terrigenous-carbonate deposits of the Middle-Upper Devonian (D_{2+3}) are observed (Fig. 3a).

Based on drilling 30 km north-west of the thermal springs, the thickness of the permafrost is 300–400 m. Overall, the Chernyshev ridge is characterized by sporadic permafrost, which is linked to the discharge of thermal waters. Up to 30–50% of the area of the watersheds is occupied by discontinuous taliks, under which the permafrost is up to 20–40 m thick. Continuous taliks are observed in the river valleys and streams. Therefore, the hydrothermal system received limited infiltration, unevenly distributed across the area.

The groundwater aquifers are associated with the carbonate strata of Silurian-Lower Permian deposits ($S\text{-}P_1$). These deposits contain heterogeneous clusters of groundwater located in porous-fractured and fractured collectors. The fracture zone usually spreads to a depth of 300–350 m. Groundwater replenishment is mainly due to local precipitation and infiltration. However, it is possible that the aquifers of the Ural fold region, which located 150 km to the east (Fig. 2) at an absolute elevation of 1500 m, are an additional source of water.

Groundwater to a depth of 300–400 m exhibits salinity of 0.3–0.5 g/L and contains $Ca–Mg–HCO_3$ (Sidorenko, 1970). The salinity in oil wells located 20–30 km north of Pymvashor ranges from 74 to 165 g/L (Derevyanko and Zharkov, 1987). In oil wells 150 km to the west at 0.8–1.5 km depth, TDS ranges from 5 to 20 g/L, increasing with depth to 50–200 g/L. The temperature of the groundwater ranges from 1.2 to 79 °C at depths of 0–3.4 km (Mamedov, 2005), implying a geothermal gradient of approximately 2.3 °C/100 m (Fig. S1).

The 8 thermal and 2 cold water sources and the connected travertine deposits discussed in this work are confined to the straight section of the V-shaped valley of Pymvashor creek (a tributary of the Adzva River) crossing a neotectonic uplift of Lower Carboniferous carbonate rock (Figs. 2 and 4). All active hot springs

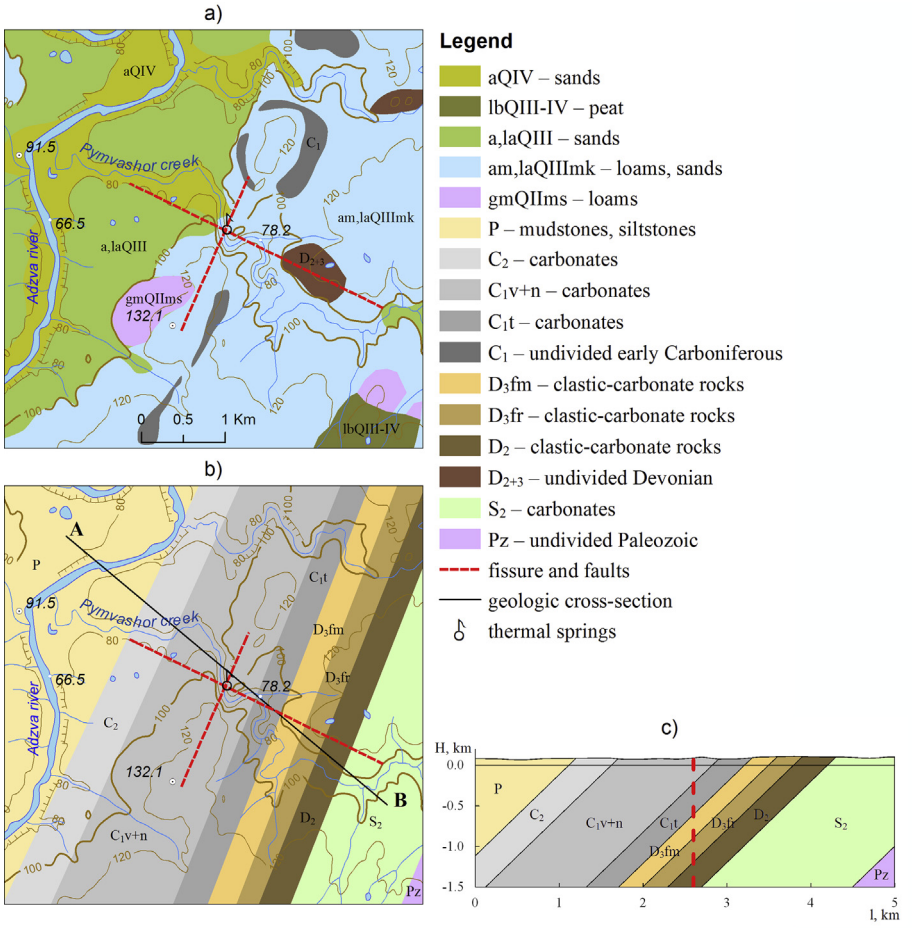

Fig. 3. Geological structure of the study area: a) map of Quaternary deposits; b) geological map; c) geological cross-section along the line AB. Modified after Vollosovych and Knyazev, 1956.

in this valley are at altitude 77–85 m.a.s.l. This section of the creek coincides with a general spreading of rock layers linked to the linear uplift of carbonate rocks (Figs. 2a and 3). This suggests that the ascent of thermal waters to the surface occurs along a fissure without vertical displacement (Vollosovych and Knyazev, 1956). It is possible that the thermal springs are confined to the intersections of faults running in north-eastern and north-western directions (Bogolitsin and Bolotov, 2011). These alleged faults are shown in Fig. 3.

Thermal source number 1 (Fig. 2b), which was depositing the travertine, ceased to operate prior to the first observations of the site in 1835 (Benjamin, 1849). Travertine deposits 3 m thick are located at the altitude of 95–88 m.a.s.l., covering the valley slope over 15 m. Thermal source number 2 (Fig. 2b), also no longer functioning, was located 20 m downstream from source No 1. Until 1955 it was discharging at 0.3–2 L/s at a temperature of 29 °C (Vollosovych and Knyazev, 1956).

The cold springs are located within the calcareous sediments of upper floodplain terraces. They discharge within the borders of these terraces and the floodplain.

3. Material and methods

3.1. Sample description and preparation

Water was sampled in December 2011 and travertine in 2010 and 2011. Sample locations are shown in Figs. 2 and 5. Information about the samples is shown in Table 1. All water samples were filtered through 0.45 μm acetate cellulose in the field. Filtered solutions for cation and trace element analyses were acidified with double-distilled HNO_3 (pH < 2); samples for anion analysis were not acidified.

3.2. Analytical procedures

Water temperature, pH, and DO were measured in the field using portable HANNA instruments with uncertainties of 0.1 °C, 0.05 pH units, and 5%, respectively. Calcium, magnesium, sodium, and potassium concentrations were determined with an uncertainty of 1–2% using an atomic absorption spectrometer (AAS) (Perkin–Elmer 5100 PC). Alkalinity was measured by potentiometric titration with HCl by automated titrator (Metrohm 716 DMS Titrino) using the Gran method (detection limit 10^{-5} M, uncertainty 2%). Major anion concentrations (Cl, SO_4) were measured by ion chromatography (HPLC, Dionex ICS 2000) with an uncertainty of 2%. Major and trace element were determined without preconcentration by inductively coupled plasma mass spectrometry (ICP-MS) (Agilent 7500ce). Good agreement (≤10%) between measured and certified U concentration in a certified river water sample (SLRS-5) was achieved.

Determinations of uranium and thorium isotopes in groundwater were made in accordance with (Malyshev et al., 1999b), as also described in Fröhlich (2013). Measurements of uranium isotopes in travertine were made in accordance with (Malyshev et al.,

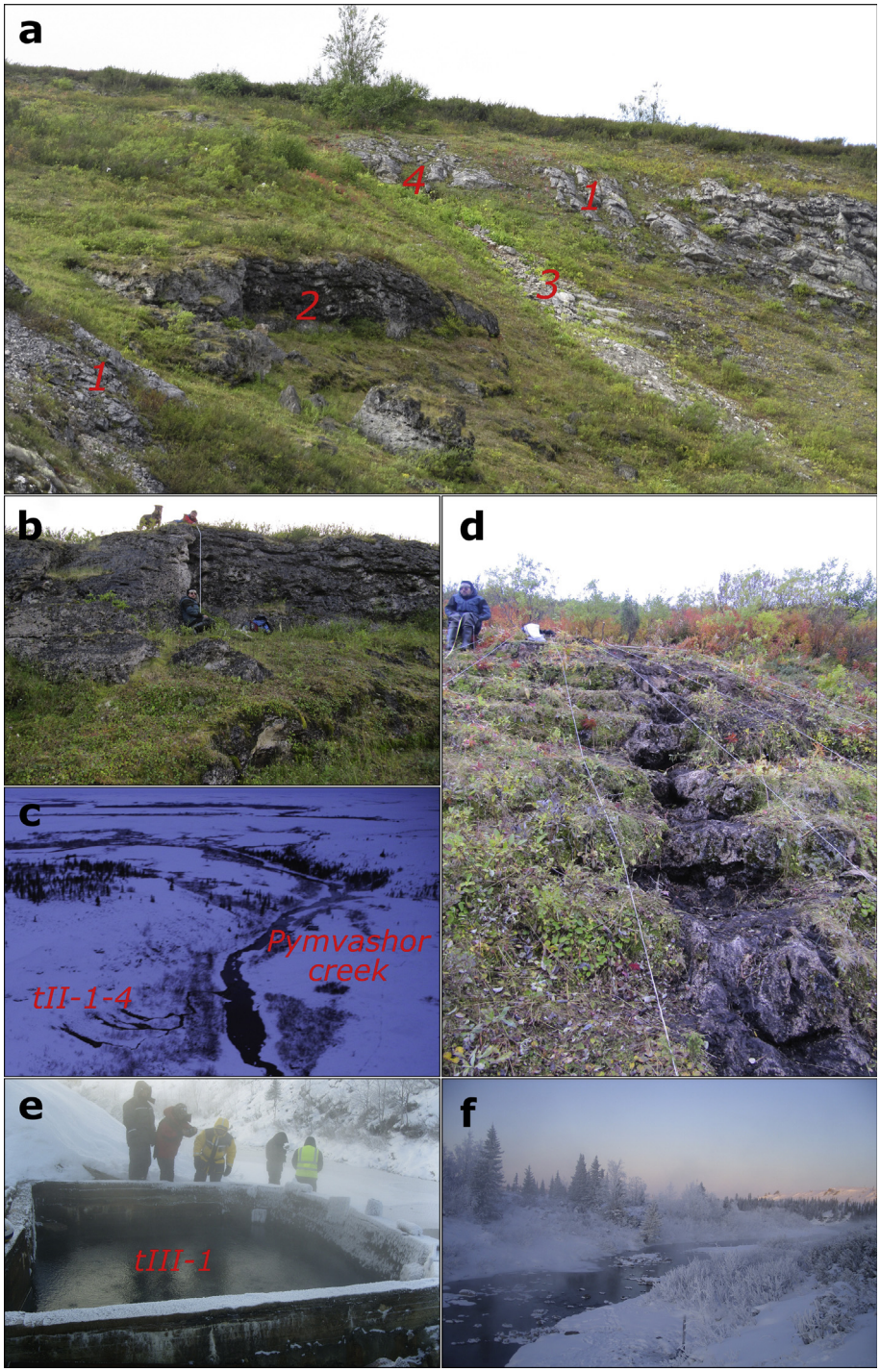

Fig. 4. Travertine and thermal springs of the studied area: a) 1 – outcrops of Lower Carboniferous limestones, 2 – outcrops of old travertine, 3 – deposition of young travertine from the springs No 2 in the form of thin (5–10 mm) crusts, 4 – location of the non-functioning springs No 2; b) outcrops of old travertine; c) thermal springs tII-1,2,3,4 and Pimvashor creek; d) travertine terraces; e) thermal springs tIII-1; f) Pimvashor creek below thermal springs tIII-1.

1999a), as described in the Supplementary Information S4. Measurements of thorium isotopes in travertine were made according to published procedures (Instruction number 448-NP, 1995), as described in the Supplementary Information S5. Spectrometric detection of alpha particles was performed using an alpha spectrometer ("Progress-alpha", uncertainty 5–6% (Th) and 10–20% (U)). Total error of analysis is defined by $\delta = \delta st + \delta sys$ (statistical + systematic). Measurement uncertainties for U and Th are reported individually (Tables 3 and 4). Efficiency of ^{232}U and ^{234}Th extraction was 40–50%.

Measurement of ^{2}H and ^{18}O was carried out using on Picarro L-2120i infrared laser spectrometer. The results are given in form of $\delta^{2}H$ and $\delta^{18}O$ in per mille relative to the Vienna Standard of Mean Ocean Water (V-SMOW). Internal lab standards, which were calibrated by the V-SMOW2, GISP, and LASP standards of the IAEA, and by the USGS45 and USGS46 standards of the American Geological Society, were used for calculation of ^{2}H and ^{18}O in samples. Accuracy was ±0.1‰ for $\delta^{18}O$ and ±1‰ for $\delta^{2}H$.

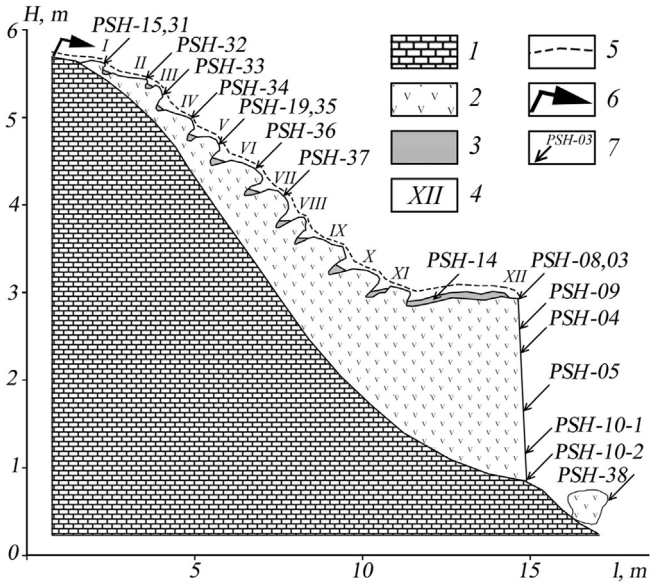

Fig. 5. Travertine sampling location. 1 – Lower Carboniferous limestones, 2 – travertine, 3 – buried alluvium, 4 – travertine terraces numbers, 5 – soil, 6 – the discharge of thermal waters in the past, 7 – sampling location travertine with their numbers.

Water samples for ^{14}C analysis were treated with carbonate-free $CaCl_2$ and NaOH solutions to precipitate Ca carbonate. Determination of ^{14}C involved dissolution of carbonates with hydrochloric acid following Arslanov et al. (1993). The resulting carbon dioxide was sintered with lithium to form lithium carbide, which was decomposed with water to produce acetylene. This was then distilled to yield benzene. Measurement of ^{14}C was made using a liquid scintillation spectrometer Quantulus 1220 (Background ^{14}C is 0.15–0.20 counts per minute, 75% counting efficiency). Measurement uncertainties for ^{14}C (as percent modern carbon, pmC) are reported individually (Table 3) and ranged from 1.9 to 9.5%.

4. Results

4.1. Chemical composition of groundwater

The composite chemical data for the thermal and cold springs at the Pymvashor site are listed in Table 2, S1 and S2. Table 2 also provides the groundwater results for oil wells C-1 and 49 (the depth of the sampling intervals 720–1028 and 3383–3389 m, respectively), which are located 150 km to the west (Mamedov, 2005). Across the dataset, the temperatures in the springs ranged from 1.6 to 28.5 °C, the pH ranged from 7.5 to 8.5, the TDS ranged from 438 to 2057 mg/L, and the DO ranged from 3.1 to 7.7 mg/L. In deep wells, the temperature ranged from 29.5 to 79 °C, the pH ranged from 7.5 to 8.45, the TDS ranged from 7.1 to 198.1 g/L, and DO = 0. Overall, as the water temperature increased from cold (1.6–2.8 °C) to warm (20.3–28.5 °C) and hot (79 °C) environments, the TDS and pH increased, and DO decreased. The concentrations of the major constituents are summarized in Fig. 6, S1 and S2. Overall, four types of groundwater were identified according to their major composition as follows: Na–Ca–HCO_3–Cl dominated (type I, Sample kII-3) and Na–Cl–HCO_3 dominated (type II, Sample kIII-1) in cold waters; Na–Cl dominated (type III, Sample kI-1,2,3; kII-1,2,3,4; kIII-1; C-1) in warm waters and Na–Ca–Cl dominated (type IV, Sample 49) in hot brines. The fresh water flow through deep portions of the aquifer mixes with the brines and then is discharged in the form of hot springs. In the near-surface horizons, the thermal water mixes with cold water, altering its composition.

The results of the geochemical analysis are briefly summarized below for different spring water sources.

4.1.1. Cold springs

Shallow groundwater in contact with carbonate deposits has a HCO_3–Ca–Mg composition. Therefore, the Na–Ca–HCO_3–Cl composition of water source kII-3, which has Na/Cl and Mg/Ca molar ratios of 0.96 and 0.43, respectively, demonstrates the influence of thermal waters (i.e., Na/Cl and Mg/Ca molar ratios of 0.90 and 0.60). The impact on the Na–Cl–HCO_3 composition of water source kIII-1 is more tangible, and the Na/Cl and Mg/Ca molar ratios of this source are 1.29 and 1.90, respectively (Table 2).

A comparison of the chemical compositions of thermal and cold waters indicates that the cold water from source kII-3, in which TDS = 438 mg/L and a Cl^- concentration = 95 mg/L, could be formed by mixing thermal water from the hot springs, which has an average TDS = 1932 mg/L and a Cl-concentration = 936 mg/L, with the cold water end member formed during the interaction of infiltrating Cl^--poor meteoric water with carbonate rocks of the aquifer. Therefore, the composition of the initial cold water can be determined using a mixing diagram. The results of the calculations indicate that water source kII-3 involved ~91% cold water end member, which has a TDS of 291 mg/L and a Cl-concentration of 16.5 mg/L, and ~9% water from the thermal springs (Supplementary Information S6, Fig. S3, Table S3).

The chemical composition of the kIII-1 source differs from that of the kII-3 source. Mass balance calculations (Supplementary Information S6, Fig. S4, Table S4) suggest that kIII-1 may be formed by mixing of thermal water with a HCO_3–Na cold water end member with a TDS of 231 mg/L in a ratio of 1:4. The HCO_3–Na composition is typical of the near-surface groundwater in the

Table 1
Information on the sampling of the thermal waters and travertine.

Type of analysis	Number of samples	Sample volume	Laboratory of analysis
Thermal water			
Major and trace element	8	10 mL	GET, Toulouse France
Alkalinity	10	50 mL	
Major kations, anions, and DOC	10		
^{14}C, $\delta^{13}C$	3	100 L	SPSU, IHMC RAS, St. Petersburg
^{238}U, ^{234}U	5	20 L	IEPN UB RAS, Arkhangelsk
δ^2H, $\delta^{18}O$	8	5 mL	SPSU, St. Petersburg
$\delta^{13}C$, $\delta^{18}O$	1	120 mL	GIN RAS, Moscow
Travertine			
^{238}U, ^{234}U	18	0.5 kg	IEPN UB RAS, Arkhangelsk
^{230}Th, ^{232}Th	5	0.5 kg	IEPN UB RAS, Arkhangelsk
$\delta^{13}C$, $\delta^{18}O$	8	0.5 kg	GIN RAS, Moscow
The chemical composition	1	50 g	NAFU, Arkhangelsk

Table 2
The main components of the chemical composition of groundwater.

Sample no	Coordinates latitude/longitude	T (°C)	Discharge (L/s)	pH	DOC (mg/L)	DO	TDS	Cl^-	HCO_3^-	SO_4^{2-}	Na^+	Ca^{2+}	Mg^{2+}	K^+	Na/Cl (mol)	Mg/Ca	10^3 Br/Cl	Water type
tI-1	N67°09′42″ E60°51′8.3″	20.3	0.7	7.6	2.0	4.5	1842	897	149	119	517	100	38.9	11.0	0.89	0.64	0.79	Na–Cl (type III)
tI-2	N67°09′41.6″ E60°51′9.8″	20.5	2.6	7.5	0.8	3.9	1849	881	168	117	516	103	38.4	10.8	0.90	0.61	0.80	
tI-3	N67°09′41.8″ E60°51′7.3″	21.7	0.28	7.6	7.0	3.5	1836	874	172	110	509	107	38.6	10.7	0.90	0.59	0.81	
tII-1	N67°09′44.1″ E60°51′04.6″	26.7	2.5	8.5	3.6	4.3	2013	967	169	129	566	112	41.4	11.6	0.90	0.61	0.87	
tII-2	N67°09′44.7″ E60°51′04.6″	25.7	1.89	8.1	7.2	4.2	2057	980	155	171	572	115	42.1	11.7	0.90	0.60	0.86	
tII-3	N67°09′44.5″ E60°51′4″	27.4	1.43	8.0	9.2	4.8	1987	956	166	127	557	118	41.4	11.5	0.90	0.58	0.88	
tII-4	N67°09′43.9″ E60°51′4.3″	27.4	1.84	8.1	1.8	4.3	2010	969	169	129	562	117	42.4	11.8	0.89	0.60	0.87	
tIII-1	N67°09′50.5″ E60°51′5.7″	28.5	13.9	7.8	1.7	3.1	2001	960	171	128	560	119	41.4	11.8	0.87	0.57	0.88	
kI-3	N67°09′38.5″ E60°51′13.9″	2.8	0.09	7.5	*NA*	7.7	438	95.1	183	27.3	61.2	49.8	13.1	0.41	0.96	0.43	*NA*	Na–Ca–HCO_3–Cl (type I)
kIII-1	N67°09′55.4″ E60°51′16.1″	1.6	4.23	7.5	*NA*	5.65	588	178	193	25.7	153	14.2	16.4	1.59	1.29	1.9	*NA*	Na–Cl–HCO_3 (type II)
Oil well C-1	N67°35′37.6″ E57°15′20.8″	29.5	0.4 (L/s·m)	7.51	*NA*	0.68	7084	4128	232	14.9	2435	186	46.7	10.6	0.91	0.41	1.6	Na–Cl (type III)
Oil well 49	N67°35′35.9″ E57°14′17.8″	79	NA	8.45	*NA*	*NA*	198,106	120,266	267	434	59,350	13,627	972	2071	0.76	0.07	2.1	Na–Ca–Cl (type IV)
Sea	*NA*	*NA*	*NA*	*NA*	*NA*	*NA*	35,000	19,354	138	2712	10,759	413	1294	387	0.86	5.05	1.5	*NA*

NA not analyzed; Oil wells C-1, 49 – from Mamedov (2005); Sea (mg/kg)- from Riley and Skirrow (1965).

Fig. 6. Changes in the Cl^-, HCO_3^-, Na^+ and Ca^{2+} content (meq/L%) with groundwater evolution from cold water to warm groundwater and brines at the study area. The amounts of anions and cations taken as 100%. The amounts of anions and cations taken as 100%.

sandy–clay aquifers of the Pleistocene and reflects the hydrolysis of aluminosilicates (Shvartsev, 1991, 2007). According to our data, this water is encountered in the taliks near the village of Karatayka, which is located in the permafrost zone northwest of the Pymvashor sources. Na–HCO_3-rich shallow groundwaters are also found in sandy–clay Vendian aquifers in areas with kimberlites formation that are north of Arkhangelsk in northwestern Russia (Malov et al., 2009; Table S5).

4.1.2. The results of thermodynamic modeling

The mineral saturation indices (*SI*) of water samples were calculated using Geochemist's Workbench Version 9.0 (Bethke and Yeakel, 2013) and SOLMINEQ-88 (Perkins et al., 1990). The saturation index is defined as $SI = \log(Q/K)$, where Q is the reaction quotient (or ion activity product) and K is the equilibrium constant at a given temperature and pressure. At equilibrium, $Q = K$ and $SI = 0$. In this case, water is in equilibrium with the mineral and no dissolution or precipitation should take place. $SI > 0$ indicates that the solution is supersaturated with respect to a given mineral; $SI < 0$ indicates undersaturation. Mineral saturation indices for calcite, aragonite, dolomite, magnesite, gypsum, and anhydrite are displayed in Fig. 7. The saturation indices indicate that the geothermal waters were saturated and supersaturated with respect to calcite, aragonite, dolomite, but undersaturated with respect to gypsum, anhydrite and magnesite. Cold waters (springs kII-3 and kIII-1) were undersaturated with respect to all minerals. Groundwater was greatly undersaturated with respect to U minerals, such as rutherfordite (UO_2CO_3), uranyl hydroxide ($UO_2(OH)_2$), and uranium oxide (UO_3) (*SI* from −2 to −9.4) (Table S6).

4.1.3. Geothermal waters

All geothermal waters of the Pymvashor springs had similar compositions with very little difference in the cation concentration. Previous studies of the Pymvashor thermal spring indicated that the $Br/10^{-3}Cl$ (ppm) ratio is between 1.8 and 1.9 (Mityusheva et al., 2011), the Na/Cl (mol) ratio ranges from 0.89 to 0.90 and the Ca/Cl (ppm) ratio is equal to 0.12 (Table S2), which may reflect the participation of deep brines in their formation. These brines, which are located >1.5 km deep, are enriched in Ca and depleted in Na, Mg and SO_4 relative to concentrated seawater (see Supplementary Information S7, Table S7).

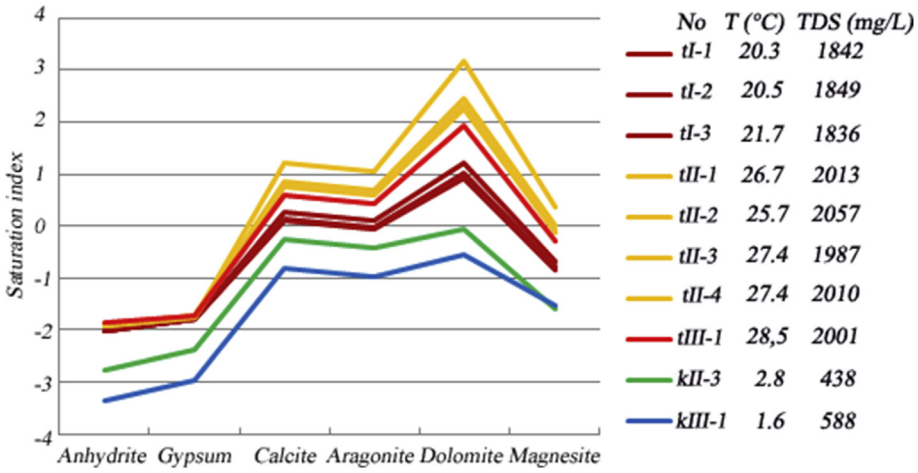

Fig. 7. Equilibrium states between major minerals of the study area and water samples.

As a result of the rise and discharge of thermal waters on the surface, the brine seeps from below and mixes with fresh water, which flows through the deep portions of the aquifer (Fig. 1). The results of the mass balance calculations indicate that the final fluid is composed of 1 part brine and 130 parts cold water end member with a TDS of 291 mg/L (Fig. S5, Table S8). The metamorphosed brines, which were collected from well 49, exhibit a relatively high calcium concentration and a low sodium concentration (Fig. 6 and S5). Therefore, the calculated concentrations of Ca^{2+} in the mixture was 34 mg/L more than that in the water from the thermal springs. In addition, the Na^{+} content was 77 mg/L less, and the Mg^{2+} content was 21 mg/L less. This result agrees with the thermal water supersaturation state with respect to calcite but is undersaturated with respect to magnesite (Fig. 7). Therefore, precipitation of calcite and dissolution of magnesite may occur in the aquifer. In addition, hydrolysis of the sodium aluminosilicates may be accompanied by precipitation of secondary clay minerals (Shvartsev, 1991, 2007). The estimated concentration of sulfate in the mixture is 97 mg/L lower than that in the thermal water sources. Therefore, dissolution of gypsum inclusions occurs, which is in agreement with the thermal waters SI with respect to gypsum (Fig. 7). However, no saturation with gypsum was achieved, which is most likely due to its low content in the rocks.

4.2. Isotope geochemistry

4.2.1. The isotopic composition of thermal water

Table 3 shows the isotopic composition of the sources in the Pymvashor valley.

4.2.1.1. $\delta^{18}O$ and $\delta^{2}H$. Due to deep freeze of the soil in sub-Arctic regions in winter, groundwater is recharged by snowmelt and summer precipitation in the warmer seasons. Evapotranspiration may remove a portion of the summer rainwater when the average daily temperature is higher than +5 °C. In this case, the isotope composition of the groundwater should be lighter in ^{2}H and ^{18}O than the annual weighted mean for atmospheric precipitation. At the Pymvashor site and in the Arkhangelsk region, the isotopic compositions of fresh and brackish groundwater fit on the meteoric water line (Fig. 8). The local meteoric water line (LMWL) for the Pymvashor site was calculated from the IAEA data for the nearest GNIP monitoring stations "Pechora" and "Salekhard" to be $\delta^{2}H = 8.0*\delta^{18}O + 6.0$ ($R^2 = 0.98$, n = 94) and the "Arkhangelsk" GNIP station to be $\delta^{2}H = 8.0*\delta^{18}O + 6.2$ ($R^2 = 0.92$, n = 48).

There are no significant deviations of the data points from the GMWL on the $\delta^{2}H$ vs. $\delta^{18}O$ diagram. This result denotes lack of i) secondary isotope fractionation due to water evaporation and freezing and ii) isotope exchange of water and carbonate rocks due to thermos-metamorphism (without an "oxygen shift" in isotopic composition). Therefore, the stable isotopes in the thermal spring water indicate that they originate from meteoric water. For the Arkhangelsk region, the $\delta^{2}H$ and $\delta^{18}O$ values varied in a wide range even though the average values were close to the annual weighted mean of atmospheric precipitation (Fig. 8). At the Pymvashor site, the average $\delta^{2}H$ and $\delta^{18}O$ values are slightly lower than the annual weighted mean of atmospheric precipitation, which may be due to the influence of evapotranspiration or climate change.

4.2.1.2. ^{14}C and $\delta^{13}C$. Groundwater dating using C isotopes and the calculations involved are given in the Supplementary Information S1. Insufficient accounting for chemical processes that can change $^{14}C_0$ over the residence time of groundwater can lead to overestimation of $^{14}C_0$ by 6–21% (Supplementary Information S1, Tables S9–S11). The ^{14}C Age (cal BP) of the thermal water, determined according to the method of Han and Plummer (2013) (Supplementary Information S1), ranged from 4960 to 7870 years.

4.2.1.3. ^{234}U and ^{238}U. Across the dataset, the U content in the thermal springs ranged from 0.238 ± 0.005 to 0.330 ± 0.007 μg/L, and the $^{234}U/^{238}U$ activity ratio ranged from 3.53 ± 0.49 to 4.19 ± 0.75. The high average $^{234}U/^{238}U$ activity ratios indicate that the deep water ascends to the surface because the shallow water in carbonate rocks has low $^{234}U/^{238}U$ ratios (1.5–2, Bonotto and Andrews, 1993, 2000; Malov et al., 2009). The relatively small dispersion in the uranium-isotope composition parameters of the source waters indicates that their formation occurs in a single hydrothermal system with the same factors and processes.

4.2.2. Isotopic composition of travertine

Table 4 lists the isotopic composition of travertine in the valley of the Pymvashor creek. It is important to note that the average $^{234}U/^{238}U$ activity ratio in travertine is higher than that of thermal water (i.e., 5.2 and 3.8, respectively). In comparison to water sources, travertines have higher $\delta^{13}C$ (−5.8 and −10‰, respectively), which is most likely due to the separation of carbon isotopes between the liquid and gas phases (Ferronsky and Polyakov, 2012) where biogenic carbon dioxide is transformed according to:

Table 3
The main components of the isotopic composition of springs.

Spring no	$\delta^{18}O$ VSMOW (‰)	$\delta^{2}H$ VSMOW (‰)	^{14}C (pmC)	$\delta^{13}C$ VPDB	^{238}U[a] (ppb)	U[b] (ppb)	$^{234}U/^{238}U$[a]
tI-1	−15.4	−114	*NA*	*NA*	0.268 ± 0.055	0.278 ± 0.006	3.74 ± 0.56
tI-2	−15.5	−114	*NA*	*NA*	*NA*	0.265 ± 0.005	*NA*
tI-3	−15.3	−113	19.29 ± 0.37	−10.7	0.264 ± 0.058	0.277 ± 0.006	3.81 ± 0.61
tII-1	−15.3	−113	18.97 ± 0.90	−9.8	0.388 ± 0.067	0.239 ± 0.005	3.53 ± 0.49
tII-2	−15.5	−114	*NA*	*NA*	*NA*	0.238 ± 0.005	*NA*
tII-3	−15.5	−114	*NA*	*NA*	*NA*	0.252 ± 0.005	*NA*
tII-4	−15.8	−115	*NA*	*NA*	0.363 ± 0.096	0.330 ± 0.007	4.19 ± 0.75
tIII-1	−15.8	−114	16.00 ± 1.52	−9.6	0.218 ± 0.049	0.242 ± 0.005	4.02 ± 0.65
kIII-1	−15.7	*NA*	*NA*	−9.5	*NA*	*NA*	*NA*

VSMOW Vienna Standard Mean Ocean Water, *VPDB* Vienna Pee Dee Belemnite, *A* – measured ^{14}C activity of total dissolved inorganic carbon (TDIC), *pmC* percent modern carbon, *NA* not analyzed.
[a] Alpha-spectrometry.
[b] Mass spectrometry.

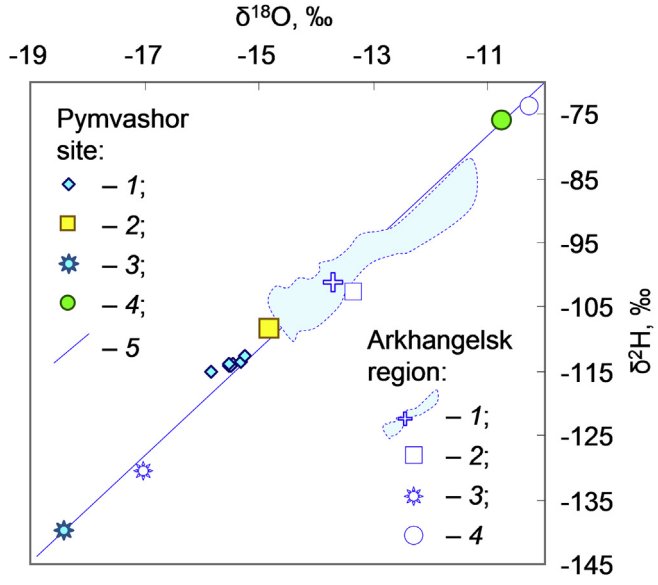

Fig. 8. Comparison of the water isotope composition in Pymvashor site with other isotope data for this region. Pymvashor site: 1 – thermal springs; 2, 3, 4 – atmospheric precipitations (weighted means calculated as average from IAEA data for "Pechora" and "Salekhard" GNIP stations for 2 – annual; 3 – cold and 4 – warm season); 5 – local meteoric water line (LMWL) from IAEA data. Arkhangelsk region: 1 – fresh and brackish groundwater (area covers the individual measurements n = 74 and cross is average); 2, 3, 4 – atmospheric precipitations (weighted mean was calculated from IAEA data for "Arkhangelsk" GNIP station for 2 – annual; 3 – cold and 4 – warm season).

$$^{13}CO_{2\,(gas)} \rightarrow H^{13}CO_3^- (water) \rightarrow {}^{13}CO_3^{2-} (water) \rightarrow {}^{13}CO_3^{2-} (solid).$$

Under normal conditions (0–25 °C), calcite is 5–6‰ richer in ^{13}C than HCO_3^- in fluid (Friedman and O'Neil, 1977; Golyshev and Padalko, 1987).

We attempted to date the travertines using the $^{230}Th/U$ method. Unfortunately, the detrital component in our samples was too high to generate reliable ages by this method. The admixture of aluminosilicates was between 3 and 4% (Table S12) with $^{230}Th/^{232}Th$ between 2.02 ± 0.10 and 4.93 ± 0.25. The only approach that provides reliable ^{230}Th ages in this case is the "isochron approach", which requires analysis of several aliquots of the same sample (Bischoff and Fitzpatrick, 1991; Ludwig, 2003; Luo and Ku, 1991). However, the analytical method used here (i.e., alpha spectrometry) does not allow us to address this problem with sufficient precision. Therefore, as a preliminary estimate of the age, we used a simplified formula for the correction of the ^{230}Th activity (Mallick and Frank, 2002) (Supplementary Information S3). The $^{230}Th/U$ age of the travertine ranged from 2460 ± 490 to 6380 ± 1270 years (Table 4). The age decreased from the top of the travertine structure to its bottom. The exception was the sample PSH4. Analyses of fossil mollusks associated with Pymvashor travertines suggest a younger age of the travertine in lower part of the deposits compared to their upper part (Bolotov et al., 2012). Modern precipitation is present as thin (5–10 mm) crusts near discharge sources and along the slope below no longer functioning source number 2, where modern travertine deposits are absent (Fig. 4a).

5. Discussion

5.1. Nature of thermal waters and evolution of the hydrothermal system

The hot springs of the Pymvashor subarctic hydrothermal system occur in an area devoid of recent volcanism. The introduction of sub-intrusive bodies accompanied by eruptions of central volcanoes occurred here prior to the Jurassic (Derevyanko and Zharkov, 1987). Therefore, endogenous formations do not affect the temperature of the thermal waters. Based on the tIII-1 thermal spring temperature of 28.5 °C and assumed thermal gradient (i.e., 2.3 °C/100 m), the circulation depth of the thermal water was estimated to be at least 1.2 km. The presence of faults allows for rapid ascent and discharge of thermal water at the surface. Thermal waters from all of the sources had similar TDS, chemical and isotopic compositions as well as a similar temperature. In addition, these parameters were nearly constant for at least 90 years based on comparison of their chemical composition from the past (Vollosovych and Knyazev, 1956) and present (Fig. 9).

U in groundwater is very sensitive to redox conditions. Under oxidizing conditions, U^{6+} is present in water in the form of uranyl carbonate complexes. Under reducing conditions, U^{4+} is precipitated as hydroxide or adsorbed onto particles of rock (Osmond and Cowart, 1982; Gascoyne, 1992; Porcelli, 2008). In addition, the isotopic composition of water reflects the balance between the α recoil effect and the dissolution rate of the host rocks (see Supplementary information S2). As shown in section 4.1.3, the fresh water flows through deep parts of the aquifers system mixing with brine and then discharges at the surface (Fig. 1). At greater depths, reducing conditions are most likely dominant, which is confirmed by the low O_2 concentrations (0.68 mg/L) and the relatively high Fe^{2+} concentration (0.3 mg/L) in sample C-1 compared to thermal water from sources exhibiting 3.1–4.8 mg/L O_2 and 0.037–0.145 mg/L of Fe^{2+}. Therefore, brine may not be a significant source of uranium. The most likely mechanism of U enrichment in the hot waters is during dissolution of Devonian deposits

Table 4
The isotopic composition and age of the travertine.

Sample no	^{238}U (ppb)	^{234}U/^{238}U	^{232}Th (ppb)	^{230}Th/^{232}Th	^{230}Th/^{238}U	U/Th age (ka)	δ^{13}C VPDB	δ^{18}O VSMOW (‰)
PSH-03	314 ± 70	5.02 ± 0.75	57 ± 3	3.83 ± 0.19	0.22 ± 0.03	3890 ± 780	−6.1	12.6
PSH-04	354 ± 71	3.59 ± 0.47	104 ± 5	2.88 ± 0.14	0.27 ± 0.04	6380 ± 1270	−6.7	12.4
PSH-05	309 ± 88	5.56 ± 0.96	75 ± 4	3.12 ± 0.16	0.2 ± 0.03	3758 ± 750	−5.8	13.5
PSH-08	386 ± 73	4.70 ± 0.75	*NA*	*NA*	*NA*	*NA*	*NA*	*NA*
PSH-09	323 ± 96	6.48 ± 1.30	*NA*	*NA*	*NA*	*NA*	−6.2	12.7
PSH-10-1	*NA*	*NA*	*NA*	*NA*	*NA*	*NA*	−5.9	12.9
PSH-10-2	443 ± 142	5.05 ± 1.26	121 ± 6	2.02 ± 0.10	0.18 ± 0.03	2460 ± 490	−6.0	12.4
PSH-14	366 ± 85	5.29 ± 1.06	*NA*	*NA*	*NA*	*NA*	*NA*	*NA*
PSH-15	386 ± 73	4.41 ± 0.71	*NA*	*NA*	*NA*	*NA*	−4.9	14.0
PSH-19	362 ± 92	5.35 ± 0.80	*NA*	*NA*	*NA*	*NA*	−5.1	13.1
PSH-21	345 ± 76	5.62 ± 0.85	*NA*	*NA*	*NA*	*NA*	*NA*	*NA*
PSH-31	413 ± 141	4.44 ± 1.11	79 ± 4	3.94 ± 0.20	0.24 ± 0.04	5850 ± 1170	−5.8	*NA*
PSH-32	377 ± 78	5.05 ± 0.75	*NA*	*NA*	*NA*	*NA*	*NA*	*NA*
PSH-33	321 ± 80	5.61 ± 1.11	*NA*	*NA*	*NA*	*NA*	*NA*	*NA*
PSH-34	476 ± 92	4.58 ± 0.91	*NA*	*NA*	*NA*	*NA*	*NA*	*NA*
PSH-35	364 ± 82	5.15 ± 0.80	*NA*	*NA*	*NA*	*NA*	*NA*	*NA*
PSH-36	332 ± 77	6.07 ± 1.18	*NA*	*NA*	*NA*	*NA*	*NA*	*NA*
PSH-37	461 ± 97	4.21 ± 0.87	69 ± 3	4.93 ± 0.25	0.24 ± 0.04	5400 ± 1080	*NA*	*NA*
PSH-38	337 ± 106	5.74 ± 1.08	*NA*	*NA*	*NA*	*NA*	*NA*	*NA*

NA not analyzed.

containing aluminosilicates, magnesite and gypsum (see sections 2 and 4.1.3). According to our calculations (see section 4.1.3 and Supplementary Information S6, Table S6), the difference in the TDS between the actual composition of the thermal springs water and the mixture brine and cold water end members is 131 mg/L. The average content of uranium in rocks in the region is 2.1 mg/kg (Smyslov et al., 1979). Therefore, during rock dissolution, 131 mg of mineral substances will be released into 1 L of water producing a U concentration of 0.275 μg/L. The actual concentration of uranium in hot springs water is close to 0.268 μg/L (Table 3). The approximate depth at which U mobilization to the fluid occurs may be close to the location of D_2 clastic sediments (i.e., 1.2–1.5 km) (Figs. 1 and 3).

The relatively low uranium content in the Pymvashor groundwater at sufficiently long aquifer residence times as well as the relatively high ^{234}U/^{238}U activity ratio (Table 3) suggest either i) high α recoil loss and low dissolution rates of the host rocks or ii) high precipitation and adsorption rate of uranium. As shown in Section 4.1, in the thermal waters that formed by mixing of fresh water end member with brines, the precipitation of calcite and hydrolysis of sodium aluminosilicates with precipitation of secondary clay minerals occur. Therefore, uranium can be adsorbed onto and/or coprecipitated with Ca carbonates and clay minerals. Higher values of the α recoil loss may be due to radioactive decay of the precipitated and adsorbed ^{238}U. As shown by Andrews et al. (1982), the decay in the adsorbed ^{238}U on the surface of fractures can produce high ^{234}U/^{238}U activity ratios in the fluid because the probability of emission of ^{234}Th and release of ^{234}U in water increases ~4-fold compared to the probability of emission directly from the rock. The increased average ^{234}U/^{238}U activity ratio in travertine compared to that in thermal waters (5.2 and 3.8, respectively) may be due to a higher contribution of brine in their mixtures with cold water end member (Table S8), which could significantly increase the saturation indices of the thermal water.

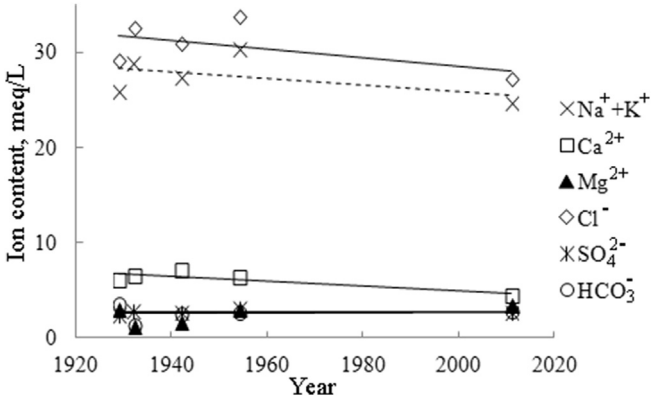

Fig. 9. Changes in the chemical composition of the thermal waters of the spring tIII-1 for years. Data for 1929, 1942 and 1954 years are from Vollosovych and Knyazev, 1956.

The hydrothermal water system began to operate due to tectonic processes. These processes created a fault through which the thermal waters could ascend and discharge at the surface under the influence of pressure gradients. Later, a recharge area was formed on a local scale. A similar process has been confirmed for the thermal springs in the Idaho batholith (USA), which discharge at discrete locations along a 50 km fault. "Stable isotopes of water, ^{14}C groundwater ages, fracture and fault orientations, fracture volume changes due to chemical evolution, and recharge area calculations suggest that the thermal springs issue from individual hydrothermal systems and that they are self-organizing" (Mayo et al., 2014, p. 25). The relatively young age of the Pymvashor thermal waters (5–7.9 ka) suggests that the area is within 5–8 km because the flow rate at depth does not exceed 1 m y^{-1} (Ivanovich et al., 1991).

The dating of thermal waters and travertine provide a minimum age for the hydrothermal system (i.e., 15.6 ka). This result represents the sum of 7.7 ka (the maximum age of travertine) and 7.9 ka (the maximum age of water). It is important to note that in nearly all hydrothermal systems described in the literature (Afsin et al., 2014; Mohammadi et al., 2010; Tan et al., 2012 etc.), thermal water mixes with shallow young water. Therefore, the residence time of the groundwater in the aquifer may be somewhat longer than that calculated in this study. However, neotectonic uplift of the Lower Carboniferous carbonate rock block on which the thermal springs are located (see above, Section 2) suggests the existence of ancient travertines, which were located above the existing deposits and destroyed by erosion. Neotectonic uplift of this block lowered the spring output from 95 to 85 m.a.s.l. Travertine deposition occurred over 12 terraces (Fig. 4d). Travertine most likely accumulated on the floodplain and the first terrace, which had a very shallow slope. After the neotectonic uplift of the carbonate block, the travertine moved continuously upwards, which created a sequence of travertine terraces, and the streambed continued to get deeper in the opposite direction. Further acceleration of

neotectonic uplift and an increase in the slope of the river valley created unfavorable conditions for travertine deposition. It is likely that the remaining large deposits of travertine formed during high past flows from source number 1 (Fig. 2b). High flows from this source resulted from the low altitude of its discharge point. After increasing to ~18 m above the creek water level, source No 1 ceased to discharge to the surface, and the deposition of travertine stopped. The thermal springs now discharge both in the floodplain and 6–8 m above creek water level without significant deposition of travertine. The deposition of travertine was observed in the form of thin (5–10 mm) crusts (Fig. 4a). However, these deposits are not preserved or accumulated due to their location on the riverbank or a steep slope (Fig. 2b).

Due to the maximum age of the travertine (7650 years) and a total rise during this period of at least 10 m, the rate of neotectonic uplift in the area of the thermal springs must be approximately 1.3 mm y^{-1}. This value is consistent with the neotectonic uplift of the northern coast of Eurasia. The highest rate was found on the Murman coast (2–6 mm y^{-1}), and the Novaya Zemlya Island rises at a rate of 2–5 mm y^{-1} (Map of recent vertical crustal movements in Eastern Europe, 1971; Nikonov, 1977, 1980).

The stable isotopic composition of the Pymvashor springs indicates that the climate during the recharge period was similar to the modern one with $\delta^2H > -150‰$ and $\delta^{18}O > -20‰$ (Fig. 8), which is typical for Holocene conditions in this region (Bowen and Revenaugh, 2003) in contrast to the Pleistocene where these parameters were $\delta^2H < -150‰$ and $\delta^{18}O < -20‰$ (Meyer et al., 2002; Streletskaya et al., 2015). This result is consistent with radioisotopic dating of the Pymvashor hydrothermal system (see section 4.2.1.2). Therefore, the $\delta^{18}O$ and δ^2H values indicate infiltration of atmospheric water into the recharge area of the hydrothermal system and suggest a stable paleoclimate in the area over the last 5–7.9 ka.

6. Conclusions

To obtain a better understanding of the nature and evolution of the thermal waters in a unique subarctic hydrothermal system located in a permafrost region, we combined hydrochemical study of thermal waters, thermodynamic modeling, hydrodynamic calculations and paleo-hydrogeological reconstructions with various isotopic analyses ($\delta^{18}O$–δ^2H, ^{14}C–$\delta^{13}C$, ^{234}U–^{238}U, and ^{230}Th–^{232}Th) to quantitatively characterize the water–rock interaction processes. This multidisciplinary approach revealed that groundwater flows through deep parts of the aquifer, mixes with brine and then discharges on the Earth's surface. The composition of the thermal water results from a mixture of one unit of the brine and 130 units of cold water end member with a TDS of 291 mg/L. According to the mass balance and thermodynamic calculations, the precipitation of calcite and the dissolution of gypsum and magnesite were accompanied by hydrolysis of sodium aluminosilicates with precipitation of secondary clay minerals occur during water–rock interaction in the aquifer.

The low uranium content in the Pymvashor groundwater at sufficiently long aquifer residence times as well as the relatively high $^{234}U/^{238}U$ activity ratios suggest a high α recoil loss and low dissolution rates of the host rocks or a high precipitation rate of uranium and its adsorption on secondary Ca carbonates and clay minerals. Elevated α recoil loss values may be due to radioactive decay of the precipitated and adsorbed ^{238}U because in this case, the probability of emission of ^{234}Th and release of ^{234}U in water increases ~4-fold compared to the probability of emission directly from the rock.

The levels of $\delta^{18}O$ and δ^2H indicate infiltration of atmospheric water into the recharge area of the hydrothermal system and a stable paleoclimate in the area over the last 5–7.9 ka. The dating of the travertines along the accumulated stream terraces allowed us to estimate the rate of neotectonic uplift in the area at close to 1.3 mm y^{-1}, which is consistent with the overall rise in the North Eurasian coast.

Acknowledgments

We are grateful to two anonymous reviewers and Associate Editor L. Aquilina for constructive comments and suggestions. This work was supported by the Russian Foundation for Basic Research, projects no. 14-05-00008_a, no. 14-05-98803_r_north_a; project NSF ARC 1204070 and grant No 14.B25.31.0001 (BIO-GEO-CLIM) of the Ministry of Science and Education of Russia. OP and MG were partially supported (25%) from RSF grant No 15-17-10009 "Evolution of the Bolshezemelskaya Tundra lake systems in the context of climate change".

Appendix A. Supplementary data

Supplementary data related to this article can be found at http://dx.doi.org/10.1016/j.apgeochem.2015.07.003.

References

Afsin, M., Allen, D.M., Kirste, D., Durukan, U.G., Gurel, A., Oruc, O., 2014. Mixing processes in hydrothermal spring systems and implications for interpreting geochemical data: a case study in the Cappadocia region of Turkey. Hydrogeol. J. 22, 7–23.

Andrews, J.N., Giles, I.S., Kay, R.L.F., et al., 1982. Radioelements, radiogenic helium and age relationships of groundwaters from the granites at Stripa, Sweden. Geochim. Cosmochim. Acta 46, 1533–1543.

Andreas, J.N., Kay, R.L.F., 1983. The U content and $^{234}U/^{238}U$ activity ratios of dissolved uranium in groundwaters from Triassic sandstones in England. Isot. Geosci. 1, 101–117.

Arslanov, Kh.A., Tertychnaya, T.V., Chernov, S.B., 1993. Problems and methods of dating of low-activity samples by liquid scintillation counting. Radiocarbon 35, 393–398.

Astakhov, V.I., Svendsen, J.I., Matiouchkov, A., Mangerud, J., Maslenikova, O., Tveranger, J., 1999. Marginal formations of the last Kara and Barents ice sheets in northern European Russia. Boreas 28, 23–45.

Benjamin, Archimandrite, 1849. Mezen Samoyeds. A. Geographical description. 2. Izhma nomadic of Samoyeds. Arkhangelsk Reg. News 4, 25–26 (in Russian).

Bethke, C.M., Yeakel, S., 2013. The Geochemist's Workbench, Version 9.0: GWB Essentials Guide. Aqueous Solutions, LLC, Champaign, Illinois, US.

Bischoff, J.L., Fitzpatrick, J.A., 1991. U-series dating of impure carbonates: an isochron technique using total-sample dissolution. Geochim. Cosmochim. Acta 55, 543–554.

Bogolitsin, K.G., Bolotov, I.N., 2011. Subarctic Hydrothermal Ecosystem Functioning in Winter. UB RAS, Yekaterinburg (in Russian).

Bolotov, I.N., Bespalaya, YuV., Usacheva, O.V., 2012. Ecology and evolution of hydrobionts in hot springs of the Subarctic and Arctic: formation of similar assemblages, adaptation of species, and microevolutionary processes. Biol. Bull. Rev. 2–4, 340–348.

Bonotto, D.M., Andrews, J.N., 1993. The mechanism of $^{234}U/^{238}U$ activity ratio enhancement in karstic limestone groundwater. Chem. Geol. (Isot. Geosci. Sec.) 103, 193–206.

Bonotto, D.M., Andrews, J.N., 2000. The transfer of uranium isotopes ^{234}U and ^{238}U to the waters interacting with carbonates from Mendip Hills area (England). Appl. Radiat. Isot. 52, 965–983.

Bowen, G.J., Revenaugh, J., 2003. Interpolating the isotopic composition of modern meteoric precipitation. Water Resour. Res. 39–10, 1299. http://dx.doi.org/10.1029/2003WR002086.

Busby, J., 2014. Geothermal energy in sedimentary basins in the UK. Hydrogeol. J. 22, 129–141.

Chalov, P.I., 1969. On the mechanism of formation of non-equilibrium relationships between the natural radioactive isotopes of uranium- and thorium-containing natural compounds. At. Energy 27–1, 26–32.

Cherdyntsev, V.V., 1955. Isotopic composition of radioelement in natural materials in connection with problems of geochronology. In: Proc. of the 3rd Session of the Commission for Determination Absolute Age of Geologic Formations. Nauka, Moscow, pp. 175–233 (in Russian).

Cuttell, J.C., Lloyd, J.W., Ivanovich, M., 1986. A study of uranium and thorium series isotopes in chalk groundwaters of Lincolnshire, U.K. J. Hydrol. 86, 343–365.

DePaolo, D.J., Maher, K., Christensen, J.N., McManus, J., 2006. Sediment transport time measured with U-series isotopes: results from ODP North Atlantic drift site 984. Earth Planet. Sci. Lett. 248 (1–2), 394–410.

Derevyanko, I.V., Zharkov, V.A., 1987. Report on Aerial Photo-geological Mapping 1:

200000 Sheet Area Q-40-XII, XVII; Q-41-I, II. Polar-Ural-Geology, Vorkuta (in Russian).
Ferronsky, V.I., Polyakov, V.A., 2012. Isotopes of the Earth's Hydrosphere. Springer, Netherlands. http://dx.doi.org/10.1007/978-94-007-2856-1-1.
Fontes, J.-Ch, Garnier, J.M., 1979. Determination of the initial activity of the total dissolved carbon. A review of existing models and a new approach. Water Resour. Res. 12, 399–413.
Fournier, R., 1989. Geochemistry and dynamics of the Yellowstone National Park hydrothermal system. Ann. Rev. Earth Planet Sci. 17, 13–53.
Friedman, J., O'Neil, J., 1977. Compilation of stable isotope fractionation factors of geochemical interest. In: Fleischer, M. (Ed.), Date of Geochemistry US, sixth ed., pp. 1–12 Geol. Surv. Prof., Pap. 440-KK.
Fröhlich, K., 2013. Dating of old groundwater using uranium isotopes – principles and applications. In: Isotope Methods for Dating Old Groundwater. IAEA, Vienna, pp. 153–178.
Fröhlich, K., Gellermann, R., 1987. On the potential use of uranium isotopes for groundwater dating. Chem. Geol. 65, 67–77.
Fröhlich, K., Ivanovich, M., Hendry, M.J., et al., 1991. Application of isotopic methods to dating of very old groundwaters: Milk River aquifer, Alberta, Canada. Appl. Geochem 6, 465–472.
Gascoyne, M., 1992. Geochemistry of the actinides and their daughters. In: Ivanovich, M., Harmon, R.S. (Eds.), Uranium-series Disequilibrium Applications to Earth, Marine, and Environmental Sciences. Clarendon Press, Oxford, pp. 34–61.
Golyshev, S.I., Padalko, N.L., 1987. Thermodynamic isotope effects in natural minerals from the approximate model of representation of frequencies. Isotopenpraxis 23, 133–139.
Han, L.-F., Plummer, N., 2013. Revision of Fontes & Garnier's model for the initial ^{14}C content of dissolved inorganic carbon used in groundwater dating. Chem. Geol. 351, 105–114.
Ingerson, E., Pearson Jr., F.J., 1964. Estimation of Age and Rate of Motion of Groundwater by the14C Method. In: Recent Researches in the Fields of Hydrosphere, Atmosphere and Nuclear Chemistry, pp. 263–283.
Instruction number 448-NP, 1995. Alpha-spectrometric Determination of Thorium Isotopes (232, 230, 228) in Soils and Rocks. RIMR, Moscow (in Russian).
Ivanovich, M., Fröhlich, K., Hendry, M.J., 1991. Uranium-series radionuclides in fluids and solids, Milk River aquifer, Alberta, Canada. Appl. Geochem. 6, 405–418.
Kamel, S., 2012. Application of selected geothermometers to Continental Intercalaire thermal water in southern Tunisia. Geothermics 41, 63–73.
Kaufman, A., Broecker, W.S., 1965. Comparison of ^{230}Th and ^{14}C ages for carbonate materials from late Lahontan and Bonneville. J. Geophys. Res. 70, 4039–4054.
Kiryukhin, A.V., Rychkova, T.V., Dubrovskaya, I.K., 2012. Formation of the hydrothermal system in Geysers Valley (Kronotsky Nature Reserve, Kamchatka) and triggers of the Giant Landslide. Appl. Geochem. 27, 1753–1766.
Kovalenko, V.I., Yarmolyuk, V.V., Bogatikov, O.A., 2009. Geodynamic setting of recent volcanism in North Eurasia. Geotectonics 43–5, 337–357.
Laverov, N.P., Kovalenko, V.I., Yarmolyuk, V.V., Bogatikov, O.A., Akinin, V.V., Gurbanov, A.G., et al., 2006. Recent volcanism of northern Eurasia: regionalization and formation settings. Dokl. Earth Sci. 410 (1), 1048–1052.
Ludwig, K.R., 2003. Mathematical-statistical treatment of data and errors for Th-230/U geochronology. Uranium-Series Geochem. 52, 631–656.
Luo, S., Ku, T.L., 1991. U-series isochron dating: a generalised method employing total-sample dissolution. Geochim. Cosmochim. Acta 55, 555–564.
Maher, K., DePaolo, D.J., Lin, J.C.F., 2004. Rates of silicate dissolution in deep-sea sediment: in situ measurement using U-234/U-238 of pore fluids. Geochim. Cosmochim. Acta 68, 4629–4648.
Mallick, R., Frank, N., 2002. A new technique for precise uranium-series dating of travertine micro-samples. Geochim. Cosmochim. Acta 66, 4261–4272.
Malov, A.I., 2013. The use of the geological benchmarks to assess the residence time of groundwater in the aquifer using uranium isotopes on the example of the Northern Dvina basin. Lithol. Min. Resour. 48, 254–265.
Malov, A.I., Kiselev, G.P., Rudik, G.P., Zykov, S.B., 2009. Uranium isotopes in the groundwater of the Vend of the Mezen Syneclise. Water Resour. 36-6, 682–691.
Mamedov, V.H., 2005. Report on the Results of Geological Exploration for the Purpose of Technical Water Supply Ardalin Oil and Gas Complex. LLC "Polar Lights", Arkhangelsk (in Russian).
Malyshev, V.I., Bakhur, A.E., Manuylova, L.I., et al., 1999a. Methods for Measuring the Specific Activity of Uranium Isotopes (234, 238) in Soils, Sediments, Rocks and Building Materials Alpha Spectrometry with Radiochemical Separation. RIMR, M (in Russian).
Malyshev, V.I., Bakhur, A.E., Manuylova, L.I., et al., 1999b. Methods for Measuring the Volumetric Activity of Uranium Isotopes (234, 238) in Natural Water Sample Alpha Spectrometry with Radiochemical Separation. RIMR, Moscow (in Russian).
Mangerud, J., Jakobsson, M., Alexanderson, H., et al., 2004. Ice-dammed lakes and rerouting of the drainage of northern. Eurasia during the Last Glaciation. Quat. Sci. Rev. 23, 1313–1332.
Map of Recent Vertical Crustal Movements in Eastern Europe. Scale 1:10 000 000, 1971. GUGK, Moscow (in Russian).
Mayo, A.L., Himes, S.A., Tingey, D.G., 2014. Self-organizing thermal fluid flow in fractured crystalline rock: a geochemical and theoretical approach to evaluating fluid flow in the southern Idaho batholith, USA. Hydrogeol. J. 22, 25–45.
Mayrhofer, C., Niessner, R., Baumann, T., 2014. Hydrochemistry and hydrogen sulfide generating processes in the Malm aquifer, Bavarian Molasse Basin, Germany. Hydrogeol. J. 22, 151–162.
Meyer, H., Dereviagin, A., Siegert, C., Schirrmeister, L., Hubberten, H.-W., 2002. Palaeoclimate reconstruction on Big Lyakhovsky Island, North Siberia – hydrogen and oxygen isotopes in ice wedges. Permafr. Periglac. Process. 13, 91–105.
Mimura, T., Oishi, K., Ogata, Y., Tokita, H., Tsuru, Y., Matsuda, K., 1995. Changes of well characteristics in the Hatchobaru Geothermal Field by exploitation of unit No. 2. In: Proc. 17th New Zealand Geothermal, Workshop, pp. 179–184.
Mityusheva, T.P., Silaev, V.I., Lavrushin, V.Yu, 2011. Travertines as a result of modern formation of minerals: evidence from the Pymvashor mineral springs. In: Mineralogical Prospects. Geoprint, Syktyvkar, pp. 236–238 (in Russian).
Mohammadi, Z., Bagheri, R., Jahanshahi, R., 2010. Hydrogeochemistry and geothermometry of Changal thermal springs, Zagros region, Iran. Geothermics 39, 242–249.
Münnich, K.O., 1957. Messungen des 14C-Gehaltes von hartem Grundwasser. Naturwissenschaften 44, 32–34.
Münnich, K.O., 1968. Isotopendatierung von Grundwasser. Naturwissenschaften 55, 3–11.
Nikonov, A.A., 1977. Holocene and Modern Crustal Movements. Science, Moskow (in Russian).
Nikonov, A.A., 1980. Modern vertical movements of the coasts of the northern and Far Eastern seas of the USSR. Geol. Geophys. 6, 71–78 (in Russian).
O'Gorman, E.J., Pichler, D.E., Adams, G., Benestead, J.P., Cohen, H., Craig, N., et al., 2012. Impacts of warming on the structure and functioning of aquatic communities: individual- to ecosystem-level responses. Adv. Ecol. Res. 47, 81–176.
Osmond, J.K., Cowart, J.B., 1976. The theory and uses of natural uranium isotopic variations in hydrology. At. Energy Rev. 14, 621–679.
Osmond, J.K., Cowart, J.B., 1982. Groundwater. In: Ivanovich, M., Harmon, R.S. (Eds.), Uranium Series Disequilibrium: Applications to Environmental Problems in Earth Sciences. Clarendon Press, pp. 202–245.
Pearson, F.J., Hanshaw Jr., B.B., 1970. Sources of dissolved carbonate species in groundwater and their effects on carbon-14 dating. Isot. Hydrol. 271–286. IAEA, Vienna.
Perkins, E.H., Kharaka, Y.K., Cunter, W.D., DeBroal, J.D., 1990. Geochemical modeling of water-rock interactions using SOLMINEQ-88. ACS Symp. Ser. 416, 117–127.
Pleshanov, A.S., Pleshanova, G.I., Shamanova, S.I., 2002. Landscape-climatic patterns of spatial distribution of refugia in the Baikal Region. Contemp. Problems Ecol. 5, 603–610.
Pointing, S.B., Bollard-Breen, B., Gillman, L.N., 2014. Diverse cryptic refuges for life during glaciation. Proc. Natl. Acad. Sci. 111–15, 5452–5453.
Porcelli, D., 2008. Investigating groundwater processes using U- and Th-series nuclides. Radioact. Environ. 13, 105–153.
Riley, J.P., Skirrow, G. (Eds.), 1965. Chemical Oceanography. Academic Press, London.
Shvartsev, S.L., 1991. The interaction of water with aluminosilicate rocks. Geol. Geophys. 12, 6–50 (in Russian).
Shvartsev, S.L. (Ed.), 2007. Geological Evolution and Self-organization of Water-rock System. RAS, Novosibirsk (in Russian).
Sidorenko, A.V. (Ed.), 1970. Hydrogeology of the USSR. V XLII, Komi ASSR. Nedra, Moscow (in Russian).
Smyslov, A.A., Moiseenko, U.I., Chadovich, T.Z., 1979. Thermal conditions and the Radioactivity of the Earth. Leningrad (in Russian), Nedra.
Streletskaya, I.D., Vasiliev, A.A., Oblogov, G.E., Tokarev, I.V., 2015. Reconstruction of paleoclimate of Russian Arctic in late Pleistocene-Holocene on base of isotope study of ice wedges. Earth's Cryosphere XIX (2), 98–106.
Svendsen, J.I., Alexanderson, H., Astakhov, V.I., et al., 2004. Late Quaternary ice sheet history of northern Eurasia. Quat. Sci. Rev. 23, 1229–1271.
Tan, H., Zhang, W., Chen, J., Jiang, S., Kong, N., 2012. Isotope and geochemical study for geothermal assessment of the Xining basin of the northeastern Tibetan Plateau. Geothermics 42, 47–55.
Vollosovych, K.K., Knyazev, S.A., 1956. Geological Investigations in the Northern Part of the Chernyshev Ridge in the Summer of 1954. Pechora-Coal-Geology, Vorkuta (in Russian).